Reluctance-Based Modular Active Damper for Chatter Suppression in Boring Bars With Different Overhangs

Asier Astarloa, Fagher Wahab, Iker Mancisidor, Maria Helena Fernandes, Iñigo Etxaniz, and Jokin Munoa

***Abstract*—Boring operations are usually limited by chatter vibrations related to the flexibility of boring bars. The location of a passive tuned mass damper close to the tool tip is a widely proposed solution, which has demonstrated robust results. However, the main drawback of this solution is that the dampers must be tuned for a certain frequency, being a customized solution for each boring bar. Active devices can overcome this limitation due to their adaptability to changing actuation frequencies. This work describes the development of a reluctance-based modular active inertial damper for its application in the suppression of chatter vibrations in slender boring bars. The solution provides the possibility to perform chatter-free boring operations at different bar overhangs due to the important stability improvement obtained in a broad frequency range.**

***Index Terms*—Active damping, boring, chatter.**

I. Introduction

In THE manufacturing of many industrial parts, such as landing gears, energy generation shafts, or oil and gas valves, internal turning operations are required. Since the internal profile defines the external geometry of the tool, slender boring bars are employed to perform these machining operations, being prone to develop self-excited vibrations, also known as chatter [1], [2]. Invariably unwelcomed, the presence of this kind of vibration is devastating since it retards production, jeopardizes the required surface finish obtention, and decreases the life of the tool as well as the mechanical elements of the machine. Moreover, when large length (L) to diameter (D) borings ($L/D > 4$) are required, stable cuts may be impossible to perform with conventional bars [3].

Over the last decades, a multitude of studies and research have been conducted to deal with chatter problems in boring [4]. The best solution to avoid this problem is to increase the dynamic stiffness of the boring bar. This enhancement can be addressed through three different approaches: the mechanical design of the bar, the use of passive dampers, and the use of active vibration control systems. As the external geometry of the bar is defined by the hole to be machined, the stiffness enhancement cannot be addressed by increasing bar section. Therefore, solutions, such as the use of high Young's modulus materials as carbon fibre [5], as well as internal geometrical optimization [6], have been proposed. However, the improvements achieved via mechanical design are limited and the use of damping devices is preferable. Solutions based on passive dampers by the use of magnetorheological fluids [7], [8], friction dampers [9], impact dampers [10], and piezo shunts [11] have been studied in academic and research environment. Nevertheless, the most employed solution in industry is the tuned mass damper (TMD). Originally introduced by Hann [12], TMDs are an effective and robust solution for chatter suppression in boring bars. One of the disadvantages of this solution is that they must be tuned for a certain frequency and can only work in a reduced bandwidth. Indeed, boring operations are usually performed with different slenderness ratios due to the variability of the workpieces that are manufactured and the limited available space in machines. This change on the dynamics of the bars makes necessary to design a customized TMD for each bar diameter and length combination. In addition, as the majority of TMD solutions are based on elastomeric suspensions, they have a limited temperature application range, due to heat-induced mistuning.

Active vibration control devices are a well-suited solution to overcome the aforementioned limitations of TMDs, mainly for the increase of the cutting capabilities and solution robustness, of high slenderness (L/D) ratio bars. In addition, active systems offer adaptability to changes in the dynamic properties of the supporting structure, so the same solution can be suitable for different bar diameters or overhangs.

Active systems on boring bars can be classified in two groups attending the application point of the force. One option is to

Manuscript received 2 December 2022; revised 19 May 2023; accepted 23 June 2023. Date of publication 25 July 2023; date of current version 16 February 2024. Recommended by Technical Editor Hungsun Son and Senior Editor Seiichiro Katsura. This work was supported in part by the EU Horizon 2020 InterQ (958357/H2020-EU.2.1.5.1) and in part by COGNIPLANT (869931) projects. *(Corresponding author: Asier Astarloa.)*

Asier Astarloa, Fagher Wahab, Iker Mancisidor, and Iñigo Etxaniz are with the Dynamics and Control, IDEKO, 20870 Elgoibar, Spain (e-mail: aastarloa@ideko.es; fwahab@ideko.es; imancisidor@ideko.es; ietxaniz@ideko.es).

Maria Helena Fernandes is with the Mechanical Engineering Department, University of the Basque Country (UPV/EHU), 48013 Bilbao, Spain (e-mail: mariahelena.fernandes@ehu.eus).

Jokin Munoa is with the Dynamics and Control, IDEKO, 20870 Elgoibar, Spain, and also with the Mechanical Engineering Department, University of the Basque Country (UPV/EHU), 48013 Bilbao, Spain (e-mail: jmunoa@ideko.es).

Color versions of one or more figures in this article are available at https://doi.org/10.1109/TMECH.2023.3295170.

Digital Object Identifier 10.1109/TMECH.2023.3295170

act at the base of the boring bar, whereas the other one is to act at the tool tip. On the one hand, systems located at the base act in a serial way with respect to machining force path and have to withstand cutting forces and high strain energies, so that high stiffness is required for such actuators [13], [14]. Moreover, if the actuator fails, the boring bar stiffness can be compromised. The application of piezoelectric patches has been proposed as a solution to this issue [15]. On the other hand, tip acting systems work usually in parallel with respect to the machining force path, providing inertial forces to the structure close to the point with higher vibration displacement [16]. The second option applications have shown more efficient results although high force density inertial actuators are demanded for a good performance due to the space restrictions close to the tool tip.

Electromagnetic inertial actuators have been proven by the literature to be a promising option for chatter suppression by their location in flexible machine tool structures [17]. Among electromagnetic devices, Lorentz force actuators are widely applied due to their linearity [18]. However, the force density offered by these actuators is usually insufficient for their location close to the cutting point where the available space is very restricted. A significantly higher force density can be achieved by reluctance-based actuators, in which the attractive force is related to the change of reluctance when the electromagnet approaches the ferromagnetic material [19]. Despite the nonlinearity behavior of this type of actuators, reluctance-based actuators have been also proposed for chatter vibration control [20], even in boring bar applications [16], [21]. Alternatively, the combination of both force principles is sought by MICA (moving iron controllable actuator) devices, with the aim of harnessing the advantages of both methods [22].

This article deals with the design of a modular reluctance-based inertial active system for its application in large boring bars for chatter suppression. The modularity and its wide frequency bandwidth provide the possibility to apply it in different bars and slenderness values. This feature allows a different approach in workshop environment: instead of having a variety of TMD equipped boring bars, a single active damper combined with different conventional boring bars can cover the same length and diameter combinations. As large size TMD equipped boring bars are extremely expensive, the proposed solution is highly applicable in workshop environment. In order to provide the guidelines, a time domain boring mechatronic model is developed first, which is used then to define the main electromagnetic and mechanical parameters of the actuator. Finally, the actuator is experimentally verified, first at a laboratory scale for its performance validation and after in real chatter suppression cases of a boring bar at different overhangs.

II. Boring Mechatronic Model for Actuator Design

The design of an active damper requires to be aware of different factors and limitations arisen in the particular cutting case of interest. However, the literature does not offer any specific design method for those active devices and their requirements

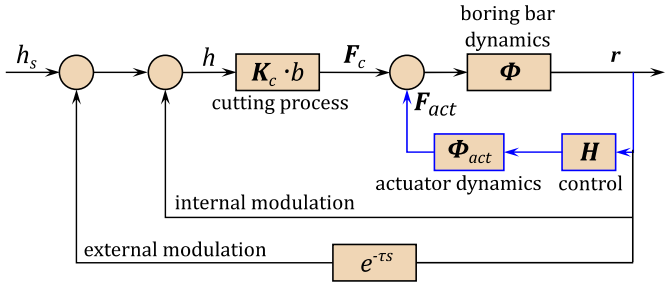

Fig. 1. Cutting process and actuation closed loops considered in the mechatronic model.

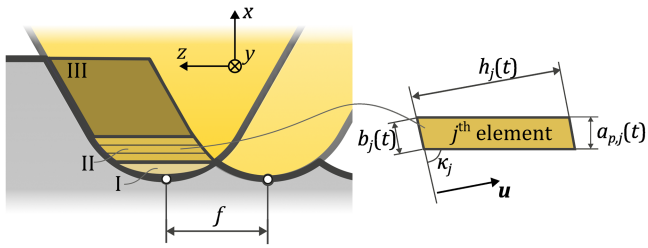

Fig. 2. Chip area discretization for nose radius consideration.

are usually defined by trial and error or based on the designer experience.

In this article, a mechatronic model is developed in order to provide guidelines in the design of inertial actuators to assure certain stability in the selected boring processes. This time domain model calculates the boring forces vector ($\boldsymbol{F}_c$) on the cutting point based on the selected cutting conditions and boring bar dynamics, whereas the effect of an inertial actuator is integrated on the loop. For that purpose, the actuation force vector ($\boldsymbol{F}_{\text{act}}$) in actuator location is calculated based on the actuator's internal configuration parameters and the employed feedback control algorithm ($\boldsymbol{H}$). The relationship between aforementioned closed loops is depicted in Fig. 1. Thereby, the model is able to provide different actuator parameters required to stabilize a specific boring process, including the actuation force, which is one of the most significant design variables for inertial actuators.

A. Cutting Forces

The chatter vibrations are known to be caused by the regenerative effect, so cutting forces must be calculated considering this dynamic effect. For that purpose, a linear cutting force is assumed wherein the cutting force depends on the chip thickness (h) and the length of the cutting edge (b)

$$\boldsymbol{F}_c = \boldsymbol{K}_c b h\,(t) + \boldsymbol{K}_e b \tag{1}$$

being $\boldsymbol{K}_c$ the cutting coefficients computed by means of the orthogonal-oblique transformation method [21] and $\boldsymbol{K}_e$ the edge coefficients. Meanwhile, b is dependent on the depth of cut of the tool (a_p) and its lead angle ($b = a_p / \sin\kappa$).

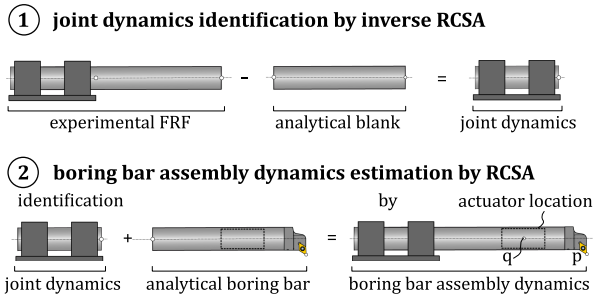

Fig. 3. Resultant boring bar FRF estimation process.

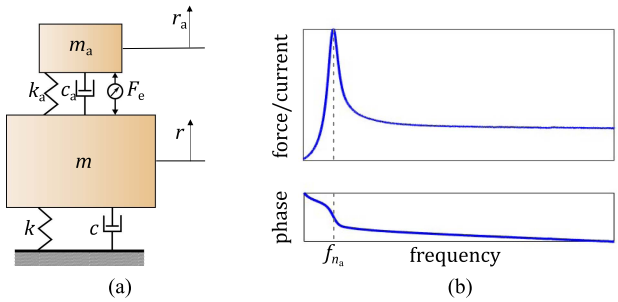

Fig. 4. Inertial active damper. (a) Lumped mass model of structure and actuator. (b) Force/current frequency response of an inertial actuator.

If a general boring process is considered, and neglecting the workpiece, the expression for the chip thickness is

$$h\left(t\right) = h_s + \boldsymbol{u}^{\mathrm{T}} \Delta \boldsymbol{r}_{\mathrm{p}}\left(t\right) \tag{2}$$

where h_s is the chip thickness due to the projection of feed per revolution ($h_s = f \sin\kappa$), $\Delta \boldsymbol{r}_{\mathrm{p}}(t)$ is the cutting point (p) (see Fig. 3) vibration vector between the previous pass and the current pass, and $\boldsymbol{u}$ is the chip thickness direction vector, that is

$$\Delta \boldsymbol{r}_{\mathrm{p}}\left(t\right) = \left\{\boldsymbol{r}_{\mathrm{p}}\left(t-\tau\right) - \boldsymbol{r}_{\mathrm{p}}\left(t\right)\right\} = \left\{\begin{array}{l} x_{\mathrm{p}}\left(t-\tau\right) - x_{\mathrm{p}}\left(t\right) \\ y_{\mathrm{p}}\left(t-\tau\right) - y_{\mathrm{p}}\left(t\right) \\ z_{\mathrm{p}}\left(t-\tau\right) - z_{\mathrm{p}}\left(t\right) \end{array}\right\} \tag{3}$$

$$\boldsymbol{u}^{\mathrm{T}} = \left\{\cos\kappa \quad 0 \quad -\sin\kappa\right\} \tag{4}$$

where $\tau = 60/N$ is the revolution period being N the spindle speed in revolution per minute. Vibration projection in the tangential direction (y) on the chip thickness is considered null, given its relatively low value with respect to the other directions.

In boring processes with large overhangs, the stability limit is in the order of the nose radius of the tool (r_ε). Therefore, for the accurate calculation of the cutting forces, it is necessary to take into account the effect of the nose radius on the chip thickness. The developed model discretizes the tool in differential elements calculating the force on each slice [23].

As it can be seen in Fig. 2, the tool is discretized in three zones. The first (I) one is the overlap zone, in which the regenerative effect does not occur, and since it is small for usual feed values, it can be neglected for force computation. The second (II) zone comprises the part of the nose radius in which the regenerative effect is present and the lead angle (κ) and consequently chip thickness projection vector ($\boldsymbol{u}$) vary. Therefore, this zone is discretized in serial elements. Finally, for depths of cut greater than the nose radius, another zone (III) is devised, where the regeneration is present and the lead angle is constant, so it can be considered as a single discrete element.

B. Boring Bar Dynamics

In order to compute the vibrations created by the cutting forces, the dynamics of the cutting point must be considered. The dynamic behavior of the boring processes is mainly defined by the first bending mode of the boring bar. However, in many cases, the clamping structure plays a key role in the overall performance.

On the one hand, the damping plays an important role on the stability of the process and hence, it is vital to provide the damping value of this first bending mode. Indeed, it is well known that the damping of mechanical structures comes from the interfaces [25], i.e., the bending mode's damping will be determined by the clamping joint. On the other hand, when two structures are mechanically connected, and the natural frequencies of their modes are similar, mode coupling can occur. As a result, a new set of pair-modes is created, mixing the shapes and increasing the damping.

Therefore, in order to obtain accurate results, the mechatronic model must consider the effect of the clamping on the dynamic behavior of the bar. This effect has been included in the estimation of the frequency response function (FRF) at the tool tip, which is used to describe the boring bar dynamics in the model.

Specifically, an hybrid receptance coupling substructure analysis (RCSA) approach has been applied [26]. In the first step, the joint dynamics are identified by means of inverse RCSA from experimental FRF measurements of blanks with different lengths. This way, by the subtraction of the dummy bar by means of analytic expressions, the dynamics of the joint are acknowledged (see Fig. 3). Then, in the second step, any boring bar can be simulated and coupled to obtain the resultant FRFs at the tool tip (p) and the actuator location (q). Thereby, the response of any boring bar can be estimated, from which the modal parameters, including the damping as well as the modal displacements, can be obtained.

C. Inertial Actuator Dynamics

Inertial actuators consist in a proof mass on which an actuation force is exerted, so that the force can be considered as a parallel loop (see Fig. 1). A diagram of an inertial actuator-based active vibration control system for 1-DOF main structure is shown in Fig. 4(a).

The mechanical interface (suspension) between main mass (m) and actuator mass (m_{a}) is represented by k_a and c_a, this is, actuator stiffness and damping, respectively. The exerted force $F_e(t)$ leads to a resulting inertial force $F_{\mathrm{act}}(t)$ on the actuator

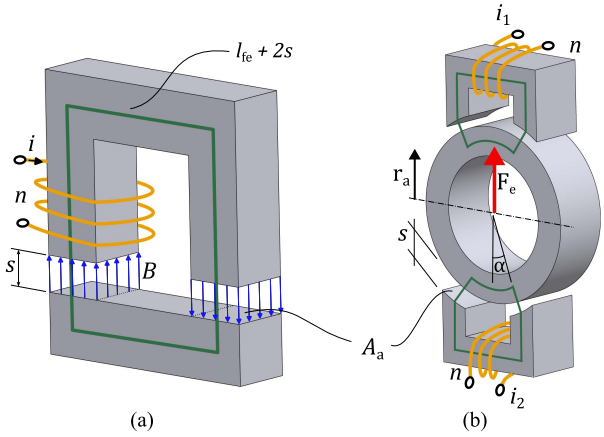

Fig. 5. Reluctance forces over: (a) clapper solenoid actuator; and (b) circular moving mass and two opposing core actuator.

location point (q) of the main structure (see Fig. 3)

$$F_{\text{act}}(t) = -c_{\text{a}}\left(\dot{r}_{\text{a}}(t) - \dot{r}_{\text{q}}(t)\right) - k_{\text{a}}\left(r_{\text{a}}(t) - r_{\text{q}}(t)\right) + F_e(t). \tag{5}$$

A typical inertial force–voltage relation in frequency domain for a general actuator acting on a fixed frame ($r_q(t) = 0$) is depicted in Fig. 4(b). As it can be observed, the suspension mode of the actuator creates an amplification on the force but involves a phase reversion of 180°, which compromises the controllability of the device. Indeed, the bandwidth of the actuator is usually limited by this suspension frequency so its reduction is generally desired.

The expression of this suspension frequency $f_{n_{\text{a}}}$ depends on actuator mass and stiffness

$$f_{n_{\text{a}}} = \frac{1}{2\pi}\sqrt{\frac{k_{\text{a}}}{m_{\text{a}}}}. \tag{6}$$

Electromagnetic technology is usually selected for inertial actuators due to its robustness and contactless force performance. The mechatronic model simulates inner electromagnetic circuits of the actuator for the calculation of the exerted force $F_e(t)$, which depends on the type of electromagnetic force principle: Lorentz or reluctance. In contrast to the forces acting on conductors in a magnetic field (Lorentz forces), the reluctance attractive force of electromagnets is generated at the boundaries between different permeabilities. The calculation of this force on a ferromagnetic material can be obtained by means of Ampere's law, which is easily understood on a simple clapper solenoid actuator [see Fig. 5(a)]

$$l_{fe}H_{fe} + 2sH_a = ni \tag{7}$$

being H_{fe}, H_a, s, n, and i the magnetic field intensity in the ferromagnetic material and in the air, the airgap, the number of turns on the coil, and the supplied current, respectively. By neglecting the reluctance of the ferromagnetic part, the magnetic field density B is approximated as linearly proportional to the magnetic permeability of vacuum $B = \mu_0 H_a$, so that the reluctance force can be calculated as

$$F_e = BH_aA_a = \frac{B^2A_a}{\mu_0} = \frac{1}{4}\mu_0 n^2 A_a\left(\frac{i^2}{s^2}\right). \tag{8}$$

Due to the attractive nature of the force, an opposite core arrangement is necessary to generate force in positive and negative directions [27]. Moreover, if a cylindrical moving element is considered, as shown in Fig. 5(b), the angle of force action line α has to be included in (8) leading to

$$F_e(t) = \frac{1}{4}\mu_0 n^2 A_a \cos\alpha\left(\frac{i_1(t)^2}{(s - r_{\text{a}}(t))^2} - \frac{i_2(t)^2}{(s + r_{\text{a}}(t))^2}\right). \tag{9}$$

Therefore, the variability of the force will be nonlinear with respect to the variable currents of both opposite cores $i_1(t)$ and $i_2(t)$ (quadratic), and the position of the proof mass $r_a(t)$ (hyperbolic). This is the main drawback of reluctance-based actuators.

As previously commented, the force capability is one of the main parameters on the design of inertial actuators, since it is usually the limiting factor of their performance. Given that the mechatronic model is based on time domain, nonlinearities, such as the actuator force limit ($F_{e_{\max}}$) or stroke limit ($r_{a_{\max}}$), can be included on the model. This way, the model enables the study of the effect of each design parameter in order to obtain the best actuator performance.

D. Control Loop

The inner electromagnetic circuit of the actuator is commanded by a controller, which calculates the amplitude and the frequency of the force to be exerted. In the case of reluctance-based actuators, the control action has two objectives. The first one is to linearize the behavior of the actuator, whereas the second one is focused on the vibration control of the main structure.

In order to linearize the magnetic force of reluctance-based actuators, a differential driving mode based on the application of a bias flux is employed. This polarization consists on the introduction of a constant magnetic flux in each ferromagnetic core in addition to a variable control flux that will be inverted in each opposing core. Considering n as a constant parameter, the flux can be controlled by the current, by introducing the next relations

$$i_1(t) = I_{\text{BIAS}} + i(t) \tag{10}$$

$$i_2(t) = I_{\text{BIAS}} - i(t) \tag{11}$$

where I_{BIAS} represents the constant current used to generate the polarization flux and $i(t)$ is the control current employed to obtain both opposing currents $i_1(t)$ and $i_2(t)$. This way, the expression of the force becomes linear with respect to the supplied control current $i(t)$ around the equilibrium position $x_a \to 0$

$$F_e = \frac{4qI_{\text{BIAS}}}{s^2}\cos\alpha \cdot i(t) + \frac{4qI_{\text{BIAS}}^2}{s^3}\cos\alpha \cdot r_{\text{a}}(t) = k_i i(t) - k_b r_{\text{a}}(t) \tag{12}$$

where $q = \mu_0 n^2 A_a/4$.

As shown in the linearized (12), the electromagnetic force is then dependent on two constants: k_i, which represents the actuator motor constant and shows that the maximum force

will be obtained when $i(t) = I_{\text{BIAS}}$; and k_b, which defines the negative stiffness of the actuator due to the bias flux. The last leads to a change in the natural frequency of the actuator when the control is activated, due to the reduction of the total stiffness with the polarization current

$$k_{\text{total}} = k_{\text{a}} - k_b;\ f_{n_{\text{a}}} = \frac{1}{2\pi}\sqrt{\frac{k_{\text{total}}}{m_{\text{a}}}}. \tag{13}$$

Nevertheless, it must be remarked that the mathematical expression (12) is no longer valid for large proof mass displacements.

Concerning the second objective related to the vibration suppression on the main structure, the control loop computes the required control current ($i(t)$) based on a control strategy ($\boldsymbol{H}(t)$). As shown in the literature, model-free feedback control strategies have shown promising results in chatter suppression applications [28]. Direct velocity feedback (DVF) algorithm based on the measurement of vibration velocity and its negative feedback multiplied by a control gain is by far the most used strategy, due to its stability when an extra damping is provided to the system.

This feedback control can be performed in the three Cartesian directions, hence resulting in a multiaxis actuation force ($\boldsymbol{F}_{\text{act}}(t)$). In addition to the feedback control, the controller transfer function ($\boldsymbol{H}(t)$) includes the signal conditioning filters. On the one hand, since accelerometers are usually used to measure the vibration on boring bars, the signal conditioning of the kinematic variable is required. On the other hand, additional filters, such as high-pass and low-pass filters, can be considered, which are commonly used in feedback control strategies in order to eliminate dc component and to attenuate high-frequency noise, respectively.

E. Numerical Resolution

The dynamical system of the complete mechatronic model is described by a matrix equation defined considering the Cartesian coordinates of both points p and q (see Fig. 3), where $\boldsymbol{M}$, $\boldsymbol{C}$, and $\boldsymbol{K}$ are the mass, damping, and stiffness matrices of the boring bar, respectively, and $\boldsymbol{r} = \{\boldsymbol{r}_{\text{p}},\ \boldsymbol{r}_{\text{q}}\}^{\text{T}}$

$$\boldsymbol{M}\ddot{\boldsymbol{r}} + \boldsymbol{C}\dot{\boldsymbol{r}} + \boldsymbol{K}\boldsymbol{r} = \begin{Bmatrix} \boldsymbol{F}_c \\ \boldsymbol{F}_{act} \end{Bmatrix}. \tag{14}$$

In order to sum the effect of both forces calculated at different points, a modal transformation is performed, being $\boldsymbol{Q}$ the modal vector matrix [29]. The columns of this matrix contain the modal displacements $\boldsymbol{\eta}$ of the modes in points p and q. That is

$$\boldsymbol{Q}^{\text{T}}\boldsymbol{M}\boldsymbol{Q}\ddot{\boldsymbol{\eta}} + \boldsymbol{Q}^{\text{T}}\boldsymbol{C}\boldsymbol{Q}\dot{\boldsymbol{\eta}} + \boldsymbol{Q}^{\text{T}}\boldsymbol{K}\boldsymbol{Q}\boldsymbol{\eta} = \boldsymbol{Q}^{\text{T}}\begin{Bmatrix} \boldsymbol{F}_c \\ \boldsymbol{F}_{act} \end{Bmatrix}. \tag{15}$$

If proportional damping is considered, the matrix equation can be decoupled for each l mode, which can be solved by numerical integration

$$\ddot{\eta}_l + 2\xi_l\omega_{n,l}\dot{\eta}_l + \omega_{n,l}^2\eta_l = \frac{1}{m_l}\left(\boldsymbol{Q}_{\text{p},l}\boldsymbol{F}_c + \boldsymbol{Q}_{\text{q},l}\boldsymbol{F}_{\text{act}}\right) \tag{16}$$

where m_l is the modal mass. Once the modal displacements have been obtained, they are projected to Cartesian reference frame in order to compute the next simulation iteration and calculate the forces again.

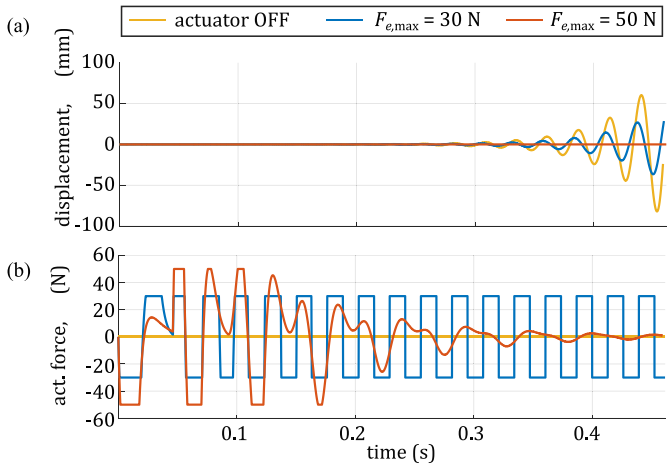

Fig. 6. Results obtained by the mechatronic model for $L/D = 14$, $a_p = 2$ mm, and $N = 1300$ r/min for different actuation force limits. (a) Radial vibration of the boring bar x_{p}. (b) Actuator's electromagnetic force $F_{e,x}$.

TABLE I
CRITICAL MODE FREQUENCY AND DAMPING ESTIMATION FOR DIFFERENT L/D RATIOS

L/D	Frequency, $f_{n_{\text{a}}}$ (Hz)	Stiffness, k (N/μm)	Damping, ζ (%)	$Q_{\text{q,x}}/Q_{\text{p,x}}$
5	294.4	41.9	1	0.69
6	232.69	34.5	1.6	0.76
8	101.4	5.73	1.2	0.84
10	72	2.44	1	0.86
12	51	3.9	0.1	0.88
14	38	1.1	0.3	0.90

TABLE II
MAIN ELECTROMAGNETIC DESIGN VARIABLES OF THE ACTUATOR

A_a (mm^2)	i_{BIAS} (A)	n (turns)	s (mm)
60 x 8.5	4	70	1

F. Mechatronic Model Results

The mechatronic model offers an intuitive interface in order to introduce all the input parameters related to the boring bar dynamics, cutting conditions, control algorithm, and actuator dynamics, including the actuation force and stroke limits. As a result, the model shows time domain charts of the cutting forces and vibrations, as well their spectra in order to define the process as a stable or unstable. Indeed, the minimum actuation force required to stabilize certain cutting process can be defined.

For instance, Fig. 6 shows the radial vibration and actuation force results obtained by the mechatronic model for the boring bar defined in Table I (slenderness case $L/D = 14$) and cutting conditions defined in Table IV, when a 2 mm depth of cut is simulated at 1300-r/min spindle speed. DVF control algorithm is used on the actuator closed loop. As shown in the figure, the process is unstable when inertial actuator inactive or its maximum force capability is too low ($F_{e,x_{\max}} = 30$ N).

TABLE III
MAXIMUM INERTIAL FORCE OBTAINED AT DIFFERENT FREQUENCIES FOR CONTROL CURRENT OF ±4 A

Frequency, ω (Hz)	Electromagnetic force, F_e (N)
40	70
80	50
120	53
160	55
200	56

TABLE IV
DEFINITION OF CUTTING TOOL AND CUTTING CONDITIONS

Cutting tool	
Boring head	Sandvik 570-SDUCR-40-11
Insert	Sandvik DCMT 11 T3 08-PM 4425
Nose radius r_ε	0.8 mm
Lead angle κ	93°
Cutting conditions	
Workpiece diameter and material	35 mm (C45k)
Feed per revolution f	0.15 mm/rev
Spindle speeds N	1300, 1400, 1700 rpm

However, it can be observed that when the actuation force can reach 50 N, the process becomes stable.

III. DESIGN OF THE RELUCTANCE-BASED ACTUATOR

A. Requirements

The first step before the design of the active solution is to define the requirements to be fulfilled by the active device. In this study, a representative case of heavy-duty boring application is sought, so that a 100-mm diameter bar with slenderness ratios up to 14 is studied. Considering that instability problems arise from slenderness ratios of 4 onwards, the solution must be able to adapt its performance to different bar overhangs. The pursued objective is to be able to achieve stable machining operations with depth of cuts up to 2 mm in all the slenderness ratios up to 14 with the tool and cutting conditions defined in Table IV.

Being an inertial actuator, it must be located onto the boring bar as closest as possible to the tool tip, whereas the outer geometry of the bar cannot be compromised due to the space restrictions of internal boring operations. In this work, the actuator location (q) will be around 120 mm away from the cutting point (p), and since the bar diameter is 100 mm, a maximum diameter of 100 mm is also stablished as requirement for the actuator. The relation between the modal displacements between both points in radial direction (x) can be also observed in Table I. Moreover, in order to be possible to adapt the actuator to different bars, it must be modular offering an standard interface both for the bar side and the tool side.

In addition, the bandwidth of the actuator must be enough to work in the bandwidth interval of the slenderness ratios. For that purpose, first the clamping dynamics were identified following the process described in Section II-B. The experimental measurements were performed with a long blank bar ($D = 100$ mm; $L = 1400$ mm) and a short blank bar ($D = 100$ mm; $L = 200$ mm) mounted on the table of the milling machine shown in Section IV. Then, the response of different

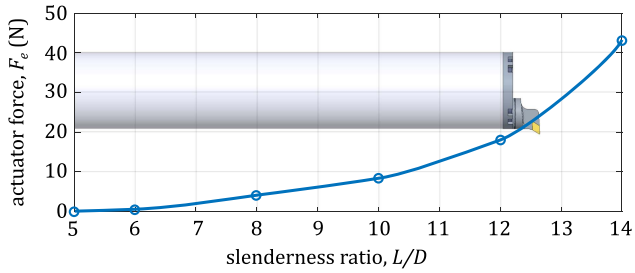

Fig. 7. Minimum actuation force required to stabilize the boring processes at different bar overhangs.

slenderness of interest was estimated [30]. Table I shows the critical first radial direction bending mode frequencies and damping values. Therefore, the actuator must cover the bandwidth around from 35 to 300 Hz.

B. Actuator Force Calculation

By knowing the main requirements for the actuator, a first estimation of the required actuation force has been obtained by the mechatronic model. Since DVF is proved to be the most efficient control strategy in poorly damped cases [28], this algorithm has been selected for the simulations, wherein the control gain and filters have been iteratively adapted to each case in order to obtain the best result. The cutting coefficients for the conditions described in Table IV have been calculated from orthogonal cutting coefficient database provided by CutPro [31].

The desired depth of cut ($a_p = 2$ mm) has been simulated for different spindle speeds, with the aim of assuring that the objective is fulfilled in all the cutting conditions. Since the bar flexibility is presented at both bending directions, a biaxial actuation seems to be the most efficient. In this way, the minimum actuation force required to stabilize the boring process at different overhangs is obtained (see Fig. 7). As expected, the most demanding case is $L/D = 14$ case, where the boring bar presents the highest flexibility. In that case, the simulation turns out a force of at least 43 N in both bending directions of the bar in order to stabilize the selected cutting conditions.

C. Electromagnetic Design

Lorentz inertial actuators have been widely proposed in the literature for chatter suppression, but the architecture offered by this type of actuators is not well adapted to cylindrical geometry of boring bars when one plane of actuation is required, so it makes hard to get a good force density and an efficient performance. Reluctance-based actuators, in addition to their higher force density, are appropriate to work in a radial geometry, as done in active magnetic bearings (AMBs).

Due to the restriction imposed by the cylindrical geometry of the boring bar, an eight-pole radial architecture similar to those present in AMB systems has been selected for the present application (see Fig. 8). In this architecture, the electromagnetic force is divided in two orthogonal directions (X,Y) composed by two opposed cores each, which follow (12) by supplying two

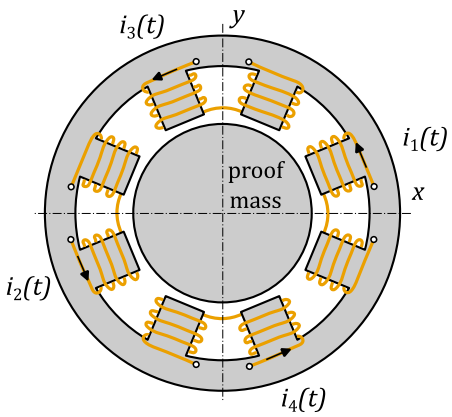

Fig. 8. Eight-pole radial architecture of the actuator.

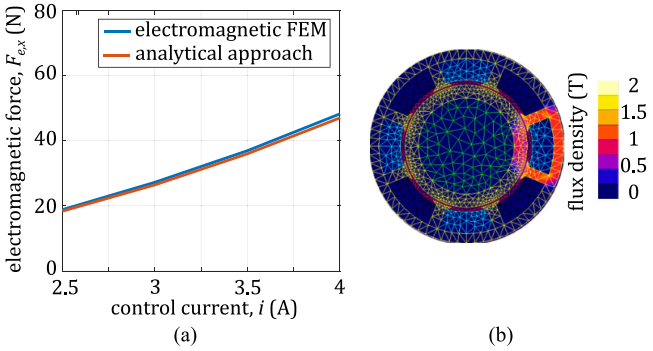

Fig. 9. (a) Comparison of electromagnetic force results in the *X*-axis obtained by the analytical approach and the electromagnetic finite element model when $x_a = 0$ and $i = I_{BIAS}$. (b) Magnetic flux density calculated by finite element software for maximum control current.

control currents $i_x(t)$ and $i_y(t)$ feeding current pairs $i_1(t)$ and $i_2(t)$ and $i_3(t)$ and $i_4(t)$, respectively.

An analytical approach has been applied to define the electromagnetic variables when dimensioning the magnetic circuit [27]. First of all, an airgap of 1 mm has been selected, which meets the assumption of low displacements of the proof mass. The angle $\alpha = 22.5^0$ is given by the geometry specifications for eight-pole architecture, whereas the pole area is calculated depending on the magnetic saturation level. In order to define the bias current, a compromise between the actuator stability and a better motor constant (k_i) must be considered. In this study, a bias current of 4 A has been defined for both directions, which fulfils the required force of 43 N [32] by varying the control currents $i_x(t)$ and $i_y(t)$ in a range of ± 4 A. Table II summarizes the main design variables to comply with the actuator requirements.

These results have been validated by means of a finite element software (FLUX), which considers local effects, such as irregular pole shoe geometries or magnetic flux losses, which are not included in the analytical approach. Fig. 9(a) shows the resultant electromagnetic force in the *X*-direction when the proof mass is positioned in the center by both the analytical approach and the finite element software. The results prove that the analytical approach is accurate enough (less than 3% error) for the primary design guidelines definition. Moreover, Fig. 9(b) shows the resultant magnetic flux density for the maximum control current, which does not saturate the actuator's core.

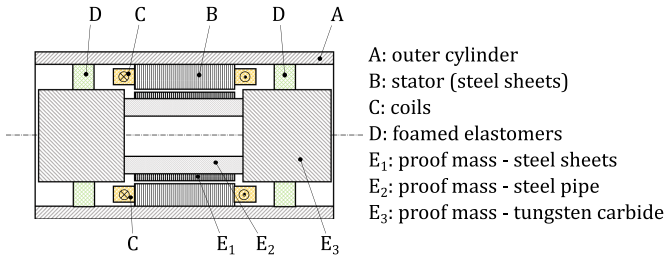

Fig. 10. Designed actuator's section view.

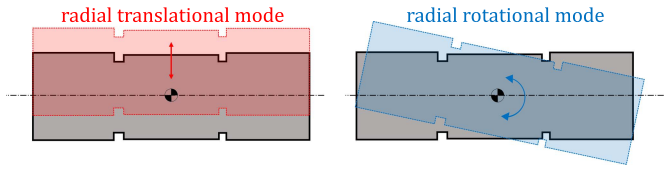

Fig. 11. Radial translational and rotational modes of the proof mass.

D. Mechanical Design

Once the electromagnetic part of the actuator has been dimensioned, the proof mass must be suspended with a mechanical device. This suspension has been made using foamed elastomers, as they offer an axisymmetric radial stiffness, combined with a reduced radial space requirement and a friction-free, wear-less operation. Fig. 10 shows a section view of the actuator, where all parts except the stator and its windings have an axisymmetric geometry. The stator is shrink fitted in the cylinder that forms the outer surface of the actuator, as well as the external surface of the foamed elastomer suspensions. Regarding the proof mass, the magnetic sheets are fitted on a hollow steel cylinder, where tungsten carbide parts are attached in each end.

In order to generate the force, the suspension mode of an inertial actuator must be lower than its actuation bandwidth. However, a suspended cylindrical rigid body shows three translational modes (two radial and one axial) and three rotational modes (two radial rotations and an axial one). As the actuation force is performed in the radial direction, the axial modes do not interact with the actuator's behavior. However, due to the cylindrical shape of the proof mass, radial rotational modes show higher natural frequency than the translational ones, and the bandwidth of the actuator can be limited by the presence of these radial rotational modes (see Fig. 11). As a solution to this issue, the proof mass has been designed in such a way that the natural frequency of the radial-translational and radial-rotational modes is equal. As a result, a new mode, which combines both motions, is generated at low frequency, suppressing beforementioned bandwidth limitation. The practical realization of this concept has been carried out by means of combining high density tungsten carbide as far as possible of the center of mass of the proof mass, and a low weight steel pipe in the middle.

During actuator operation, the flux polarization introduces a negative stiffness. Therefore, the total stiffness of the system is

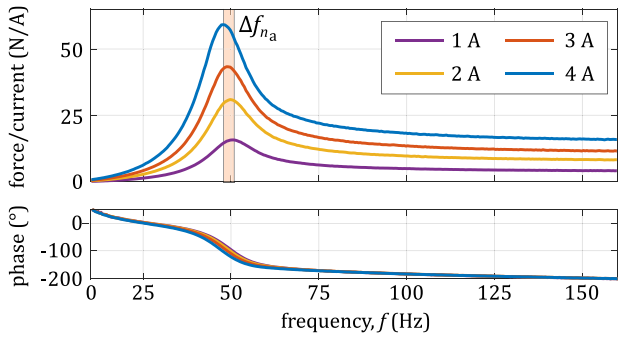

Fig. 12. Force/current relation performed by the actuator for different I_{BIAS} values, where the difference on the negative stiffness and motor constant is shown.

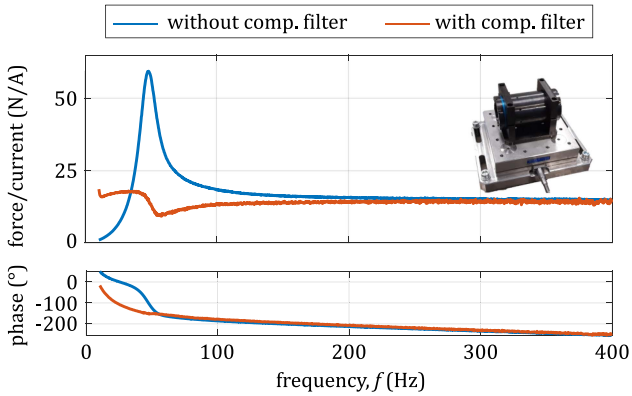

Fig. 13. Force/current relation performed by the actuator in 10–400 Hz frequency range with the maximum control current of 4 A, with the experimental validation setup where the actuator is mounted in a dynamometric plate.

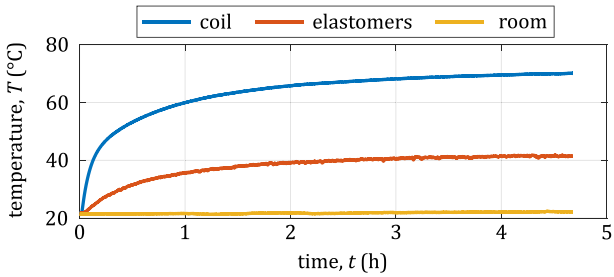

Fig. 14. Thermal validation test results.

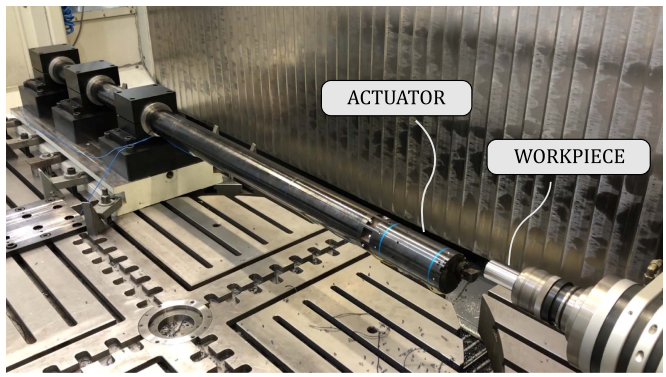

Fig. 15. Experimental setup.

the difference between the foamed elastomer's stiffness (k_a) and the flux induced negative stiffness (k_b).

By knowing the electromagnetic force performed by the actuator, the proof mass (m_a), which does not exceed the stroke limit, can be calculated. In this case, a proof mass of 4.8 kg has been selected. To comply with this mass value, the total longitude of the actuator is 200 mm. The natural frequency (f_{n_a}) of the actuator without polarization flux is 53 Hz, which is a compromise value between the desired bandwidth and avoid excessive static displacement of the proof mass. In order to comply with the previously defined bandwidth requirement (35 to 300 Hz), a compensator filter is used in the control loop to enhance the control action at lower frequencies [33]. This compensation filter substitutes the suspension frequency pole to lower frequencies and avoid the instability due to the phase shift generated by the suspension mode.

The device has been designed as a modular damper in order to offer the possibility to be attached onto different boring bars with various diameters. For that purpose, a fitting interface has been disposed on each of the actuator's ends, so that the device can be adapted to different boring bars on one side and the tool clamp systems on the other side.

IV. Experimental Validation

The experimental validation has been carried out in two stages. First, the performance of the actuator has been tested in relation to generated force, linearity, and thermal behavior. Afterward, its performance as an active chatter suppression system has been tested on a 100-mm diameter boring bar. The actuator is controlled by a programmable automation controller wherein a Simulink model is running.

A. Actuator Validation

An open-loop dynamic characterization of the actuator response has been carried out. In this way, its performance without external effects or disturbances has been tested.

First of all, the actuation force and bandwidth have been verified by mounting the actuator on a dynamometric plate (see Fig. 13). In order to validate the results provided by the linear model (12), a swept sinusoidal control current $i_x(t)$ with an amplitude of ± 0.25 A has been introduced for different bias currents. Fig. 12 shows the inertial force measured by the dynamometric plate per control current unity, where the increase of the polarization current I_{BIAS} shows the expected effects: an increase of the motor constant (k_b) and an increase of the negative stiffness, which leads to a reduction in the natural frequency of the actuator (f_{n_a}). When a bias current of 4 A is used, a natural frequency of 48.5 Hz and motor constant of 14 N/A is obtained, which agrees the results obtained on the design stage, whereas the actuator shows a stable performance. Hence, 4-A bias current has been selected for the actuator and is used henceforth.

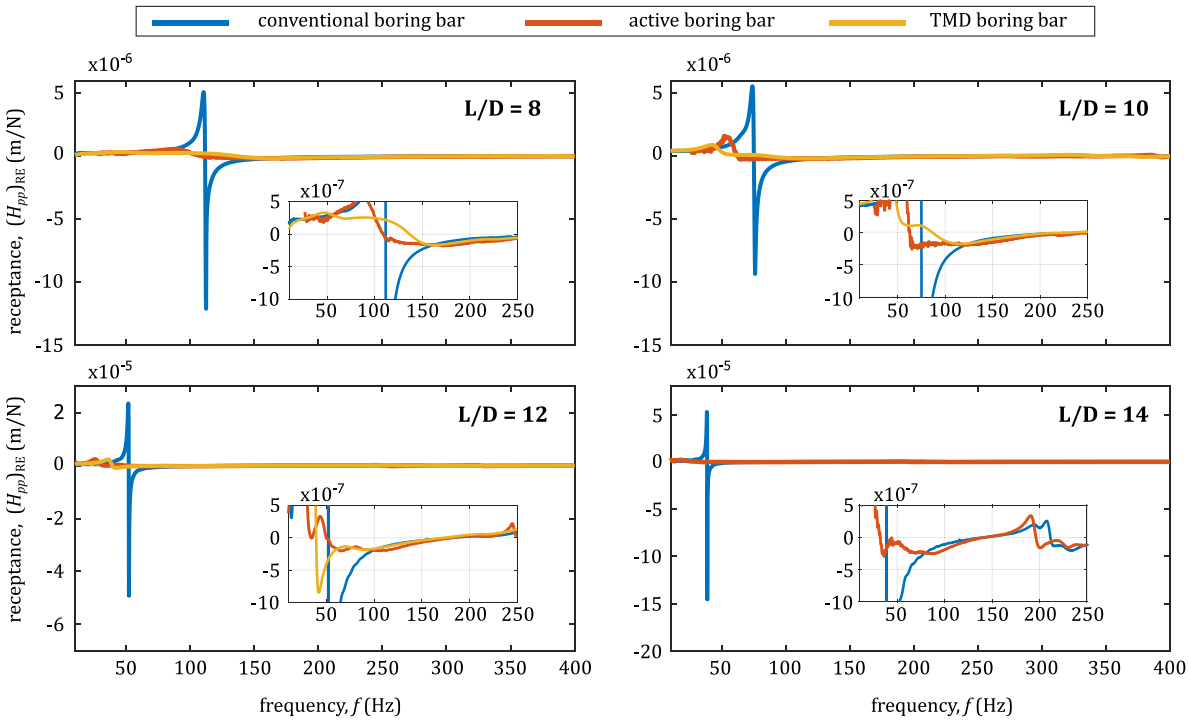

Fig. 16. Dynamic response of the boring bar without and with active damper for different bar slenderness ratios.

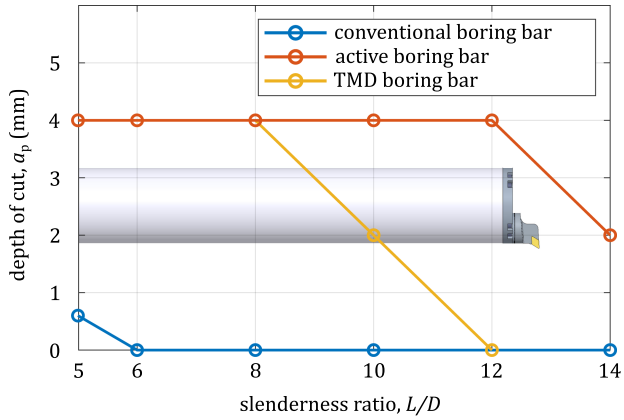

Fig. 17. Cutting tests results.

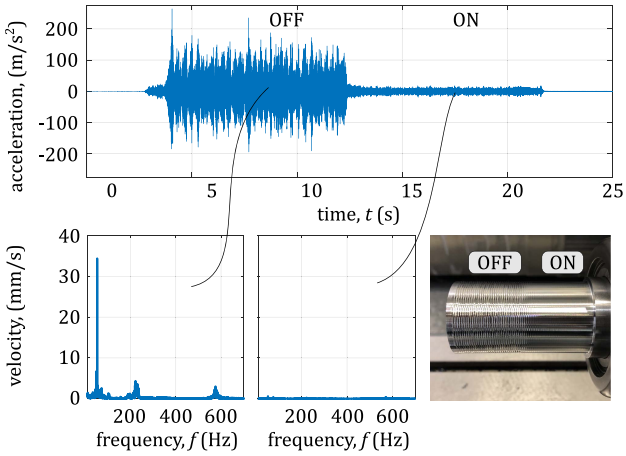

Fig. 18. Chatter suppression by means of the inertial actuator for the case $L/D = 14$, $N = 1700$ r/min, and $a_p = 0.8$ mm (measured at point p).

However, as previously commented, the actuator behavior does not comply the desired bandwidth due to the phase reversion of 180° that occurs at suspension mode frequency. Therefore, a compensation filter that locates the suspension mode pole at a lower frequency (15 Hz) has been applied by the control loop. Fig. 13 shows the actuator's response for a swept sinusoidal current (±0.25 A) from 10 to 400 Hz, where the improvement on the phase lag around the suspension frequency is visible. When the compensation filter is not used, the actuator shows a dynamic amplification due to the suspension mode at 48.5 Hz, followed by a flat and linear response for frequencies above it. The introduction of the compensation filter modifies the actuator performance around these frequencies due to the virtual modification of its suspension mode, avoiding abrupt phase changes in the frequency range of interest. Consequently, the required bandwidth can be achieved in the actuator.

Once the bandwidth of the actuator has been validated, the force capability of the actuator has been verified by introducing maximum control current amplitude (±4 A) sinusoidal signals at different frequencies, whereas the achieved force has been measured by a dynamometric plate. The results shown in Table III prove that the actuator is able to achieve more than the required force of 43 N for all the cases. The actuator's maximum power consumption will be reached when the variable current equals the bias one, resulting in 750 W.

In the second validation stage, a thermal validation has been carried out to check that both windings and foamed elastomers work within a safe temperature range. Windings must not exceed 100 °C, since higher values can compromise their insulation coating, whereas the foamed elastomers must not exceed 70 °C to avoid degradation. The test has been performed introducing a 100-Hz sine signal with the nominal bias current (4 A) and for the maximum control voltage (4 A), until thermal stabilization of the actuator has been achieved. Fig. 14 shows the result of the test, where registered temperatures do not exceed previously defined limits after more than 4-h working at the maximum capability, hence validating the actuator thermal behavior. In addition, the variation of the foamed elastomer's dynamic elastic modulus due to the increase of temperature is less than 7%. Therefore, the variation of the suspension frequency due to heat is negligible ($< 5\%$).

B. Active Chatter Suppression

Once the actuator's performance has been validated, it has been attached to the free end of the selected 100-mm diameter boring bar, being this bar clamped by split sleeves in the table of a milling machine (see Fig. 15). The machine's head has been used as a lathe spindle by mounting 50-mm diameter workpieces in a mechanical power chuck. In the performed cutting tests, the spindle head is also responsible for the cutting feed, so the bar slenderness is constant in each cutting operation. Regarding the control of the actuator, a collocated accelerometer-fed closed-loop control has been applied. Specifically, DVF control with its corresponding low-pass and high-pass filters has been used.

The boring bar has been clamped at different overhangs and the effect of the active damper has been characterized by means of FRF. As the onset of boring chatter is dependent on the minimum of the real part of the FRF in the tool tip [34], the effect of the active damper on the real part is shown in Fig. 16. The actuator can adapt its actuation to the variation of the natural frequency at different overhangs, achieving a residual real part flexibility below 0.25 μm/N for all the cases. It is noteworthy that it signifies a real part reduction of 580 times for $L/D = 14$ case. In addition, the tests have also been conducted with a same diameter TMD equipped boring bar (Sandvik 570-3C 100 1500), which is tuned for $L/D = 10$ slenderness. The comparison between both solutions shows that the proposed solution is realistic and applicable in workshop environment. Besides, the active solution behaves in all the overhangs similarly to the passive one on its nominal overhang.

In order to validate the effectiveness of the actuator, longitudinal turning tests have been carried out with and without the actuator. Machining tests have been performed under the conditions defined in Table IV. In order to cover the stability lobe effect, three different spindle speeds have been selected, so at least one of them is close to a critical spindle speed for each overhang and boring bar.

Fig. 17 shows the cutting tests' results, where the minimum stable depth of cut of all the spindle speeds is shown for each overhang and boring bar. As it was expected, the stability of the boring bar without any damper is low, being only capable of performing $a_p = 0.6$ mm chatter free cuts at 5×D overhang. Regarding the active damper, stable cuts were performed up to 4 mm until 1200-mm overhang, and 2 mm in 1400 mm. Higher depths of cut could not be tested due to the insert's a_p limitation. Passively damped boring bar showed similar behavior up to 8×D overhang, but decreasing cutting capacity was registered from 10×D overhang and above. In particular, first bending mode related chatter limited the 12×D overhang, whereas 10×D overhang was limited by a high-frequency mode chatter. This behavior has its origin in the inadaptability of the passive solutions to changes in the system's properties as natural frequency or modal mass, as they are tuned for the nominal working condition.

Fig. 18 shows the effect of the developed active damper for 14 L/D ratio case when 0.8-mm depth of cut is machined at 1700-r/min spindle speed. As it can be observed, a great improvement is achieved both at vibration level (35 times reduction) and on the surface finish of the workpiece when the active damper is switched ON.

V. Conclusion

This article presents the development and application of a biaxial reluctance-force-based active module for chatter suppression on boring operations. The dynamic properties of this type of tooling change drastically with the variation of the overhang, so the active modular solution can cover all these cases. This way, a single active damper can cover various length and diameter bar combinations, replacing the need for multiple TMD equipped bars.

A mechatronic model is developed to calculate the required actuation force as a previous step to the design process. The model includes the effect of reluctance-based actuators on the boring process forces. The nose radius is considered, as the stability limit of large overhang boring processes is, in many cases, in the order of the nose radius. This model shows that a 43-N biaxial actuator enables the suppression of chatter for the selected application.

In order to increase the actuator bandwidth, this article proposes to equal the natural frequency of the radial-translational and radial-rotational modes. Therefore, the bandwidth of the actuator is not limited by intermediate rotational mode.

The validation tests of the actuator show the fulfilment of defined requirements. Finally, the experimental application of the actuator on a 100-mm diameter boring bar has been performed, covering a wide overhang range from 5 to 14 L/D ratio. The results show a significant improvement both in the dynamic response of the bar and on the stable execution of boring operations for all the slenderness ratios. Indeed, the proposed solution permits to perform stable machining operations, which would be unfeasible to be accomplished without it.

References

[1] J. Tlusty and M. Polacek, "Beispiele der behandlung der serlbsterregten schwingung der werkzeugmaschinen," in *Proc. 3rd FoKoMa*, 1957, pp. 47–56.

[2] S. A. Tobias and W. Fishwick, "Theory of regenerative machine tool chatter," *The Engineer*, vol. 205, pp. 199–203, 1958.

[3] E. I. Rivin and H. Kang, "Enhancement of dynamic stability of cantilever tooling structures," *Int. J. Mach. Tools Manufacture*, vol. 32, no. 4, pp. 539–561, 1992.
[4] J. Munoa et al., "Chatter suppression techniques in metal cutting," *CIRP Ann.*, vol. 65, no. 2, pp. 785–808, 2016.
[5] D. G. Lee and N. P. Suh, "Manufacturing and testing of chatter free boring bars," *CIRP Ann.*, vol. 37, no. 1, pp. 365–368, 1988.
[6] M. Weck, N. Hennes, and M. Krell, "Spindle and toolsystems with high damping," *CIRP Ann.*, vol. 48, no. 1, pp. 297–302, 1999.
[7] A. Som, D.-H. Kim, and H. Son, "Semiactive magnetorheological damper for high aspect ratio boring process," *IEEE/ASME Trans. Mechatron.*, vol. 20, no. 5, pp. 2575–2582, Oct. 2015.
[8] H. Pang, F. Liu, and Z. Xu, "Variable universe fuzzy control for vehicle semi-active suspension system with MR damper combining fuzzy neural network and particle swarm optimization," *Neurocomputing*, vol. 306, pp. 130–140, 2018.
[9] S. A. Tobias, *Machine Tool Vibrations*. Glasgow, U.K.: Blackie, 1965.
[10] F. Koenigsberger and J. Tlusty, *Machine Tool Structures*. New York, NY, USA: Pergamon, 1970.
[11] A. Matsubara, M. Maeba, and I. Yamaji, "Vibration suppression of boring bar by piezoelectric actuators & LR circuit," *CIRP Ann.*, vol. 63, no. 1, pp. 373–376, 2014.
[12] R. S. Hahn, "Design of Lanchester damper for elimination of metal cutting chatter," *Trans. ASME*, vol. 73, no. 3, pp. 331–335, 1951.
[13] H. Tanaka, F. Obata, T. Matsubara, and H. Mizumoto, "Active chatter suppression of slender boring bar using piezoelectric actuators," *JSME Int. J. Ser. C, Dyn., Control, Robot., Des. Manuf.*, vol. 37, no. 3, pp. 601–606, 1994.
[14] F. Chen, M. Hanifzadegan, Y. Altintas, and X. Lu, "Active damping of boring bar vibration with a magnetic actuator," *IEEE/ASME Trans. Mechatron.*, vol. 20, no. 6, pp. 2783–2794, Dec. 2015.
[15] B. Tang, H. Akbari, M. Pouya, and P. V. Pashaki, "Application of piezoelectric patches for chatter suppression in machining processes," *Measurement*, vol. 138, pp. 225–231, 2019.
[16] B. W. Wong, B. L. Walcott, and K. E. Rouch, "Active vibration control via electromagnetic dynamic absorbers," in *Proc. IEEE Int. Conf. Control Appl.*, 1995, pp. 868–874.
[17] A. Cowley and A. Boyle, "Active dampers for machine tools," *CIRP Ann.*, vol. 18, no. 2, pp. 213–222, 1969.
[18] J. Munoa, I. Mancisidor, N. Loix, L. G. Uriarte, R. Barcena, and M. Zatarain, "Chatter suppression in ram type travelling column milling machines using a biaxial inertial actuator," *CIRP Ann.*, vol. 62, no. 1, pp. 407–410, 2013.
[19] N. H. Vrijsen, J. W. Jansen, and E. A. Lomonova, "Comparison of linear voice coil and reluctance actuators for high-precision applications," in *Proc. IEEE 14th Int. Power Electron. Motion Control Conf.*, 2010, pp. S3–29–S3–36.
[20] B. Chung, S. Smith, and J. Tlusty, "Active damping of structural modes in high speed machine tools," *J. Vib. Control*, vol. 3, no. 3, pp. 279–295, 1997.
[21] E. Abele, M. Haydn, and T. Grosch, "Adaptronic approach for modular long projecting boring tools," *CIRP Ann.*, vol. 65, pp. 393–396, 2016.
[22] F. Claeyssen, G. Magnac, and O. Sosnicki, "Moving iron controllable actuators," in *Proc. Actuator*, 2008, C3.3, pp. 1–4.
[23] E. Budak and E. Ozlu, "Analytical modelling of chatter stability in turning and boring operations: A multi-dimensional approach," *CIRP Ann.*, vol. 56, no. 1, pp. 401–404, 2007.
[24] J. Munoa, M. Sanz-Calle, Z. Dombovari, A. Iglesias, J. Pena-Barrio, and G. Stepan, "Tuneable clamping table for chatter avoidance in thin-walled part milling," *CIRP Ann.*, vol. 69, no. 1, pp. 313–316, 2020.
[25] E. I. Rivin, *Stiffness and Damping in Mechanical Design*. New York, NY, USA: Marcel Dekker, 1999.
[26] A. Astarloa, A. Comak, I. Mancisidor, M. H. Fernandes, J. Munoa, and Z. Dombovari, "Improvement of boring operations by means of mode coupling effect," *CIRP J. Manuf. Sci. Technol.*, vol. 37, pp. 633–644, 2022.
[27] E. H. Maslen and G. Schweitzer, *Magnetic Bearings*. Berlin, Germany: Springer, 2009.
[28] I. Mancisidor, J. Munoa, and R. Barcena, "Optimal control laws for chatter suppression using inertial actuator in milling processes," in *Proc. 11th Int. Conf. High Speed Machining*, HSM2014-14034, 2014, pp. 1–8.
[29] D. J. Ewins, *Modal Testing, Theory, Practice, & Application*, 2nd ed. Hoboken, NJ, USA: Wiley, 2000.
[30] A. Astarloa, M. H. Fernandes, I. Mancisidor, J. Munoa, and Z. Dombovari, "Prediction of the dynamic stiffness of boring bars," in *Proc. 9th Manuf. Eng. Soc. Int. Conf., IOP Conf. Ser.: Mater. Sci. Eng.*, 2021, Art. no. 12007.
[31] CutPro, UBC Advanced Machining Simulation System, Manufacturing Automation Laboratories, Inc., Vancouver, BC, Canada, 2000.
[32] F. Wahab, A. Astarloa, I. Mancisidor, M. H. Fernandes, I. Etxaniz, and J. Munoa, "Development of a magnetic reluctance force actuator for chatter suppression in boring bars," in *Proc. IEEE Int. Conf. Exhib. New Actuator Syst. Appl.*, 2022, pp. 1–4.
[33] I. Mancisidor, J. Munoa, R. Barcena, X. Beudaert, and M. Zatarain, "Coupled model for simulating active inertial actuators in milling processes," *J. Adv. Manuf. Technol.*, vol. 77, no. 1, pp. 581–595, 2015.
[34] Y. Altintas, *Manufacturing Automation: Metal Cutting Mechanics, Machine Tool Vibrations, and CNC Design*, 2nd ed. Cambridge, U.K.: Cambridge Univ. Press, 2012.

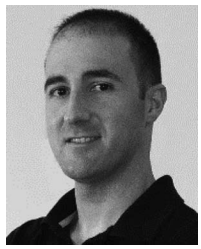

Asier Astarloa was born in Elgoibar, Spain, in 1986. He received the M.Sc. degree in mechanical engineering from the University of Mondragon, Mondragón, Spain, in 2011, and the Ph.D. degree in mechanical engineering from the University of the Basque Country, Bilbao, Spain, in 2023.

He has been an Engineer with the Dynamics and Control Group, IDEKO Research Center, Elgoibar, Spain, since 2010, specialized on diagnosis and resolution of vibration-related problems in machine tools.

Fagher Wahab was born in Bilbao, Spain, in 1989. He received the B.Sc. and M.Sc. degrees in mechanical engineering from the University of the Basque Country (UPV/EHU), Bilbao, Spain, in 2016 and 2018, respectively.

He has been an Engineer with the Dynamics and Control Group, IDEKO Research Center, Elgoibar, Spain, since 2018, specialized on active vibration control and mechatronics for machine tools.

Iker Mancisidor was born in Zumaia, Spain, in 1985. He received the M.Sc. degree in mechanical engineering from the University of Mondragon, Mondragón, Spain, in 2009, and the Ph.D. degree in mechanical engineering from the University of the Basque Country, Bilbao, Spain, in 2014.

He has been an Engineer with the Dynamics and Control Group, IDEKO Research Center, Elgoibar, Spain, since 2009, specialized on active damping solutions for the resolution of vibration-related problems in machine tools. He spent six months as a Postdoctoral Fellow with the Precision Controls Laboratory, University of Waterloo, Waterloo, ON, Canada, in 2016.

Maria Helena Fernandes was born in Caracas, Venezuela, in 1966. She received the bachelor's degree from the University Simón Bolívar, Caracas, Venezuela, in 1989, and the Ph.D. degree from the University of the Basque Country (UPV/EHU), Bilbao, Spain, in 1994, both in mechanical engineering.

She joined the Department of Mechanical Engineering, University of the Basque Country (UPV/EHU), in 1992, and is currently an Associate Professor with the Engineering School of Bilbao.

Iñigo Etxaniz was born in Urretxu, Spain, in 1972. He received the M.Sc. degree in mechanical engineering from the University of the Basque Country in Bilbao (UPV/EHU), Bilbao, Spain, in 1998.

From 1998 to 2006, he was with Fundación Tekniker on developments related with magnetic bearings. In 2007, he was with Lantier for the paper industry. In 2008, he was a Technical Manager with Obeki, an electric motor manufacturer. From 2008 to 2019, he was again with Fundación Tekniker as a test bench Project Manager. Since 2019, he has been with IDEKO, Elgoibar, Spain, as a Mechatronics Engineer.

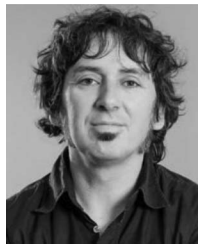

Jokin Munoa was born in Tolosa, Spain, in 1973. He received the M.Sc. degree in mechanical engineering from the University of Navarra, Pamplona, Spain, in 1998, and the Ph.D. degree in mechanical engineering from the University of Mondragon, Mondragón, Spain, in 2007.

He is specialized in vibration problem resolution in metal cutting operations based on theoretical stability models and experimental techniques. He has been a Manager with the Dynamics and Control Group since 2009 and has been a Scientific Manager since 2020 with IDEKO Research Center, Elgoibar, Spain. He has been an Associated Research Fellow with the University of the Basque Country (UPV/EHU), Bilbao, Spain, since 2020, and a Fellow Member in the International Academy of Production Engineering (CIRP) since 2021.